

AD-779 549

THEORETICAL STUDY OF DYNAMIC STALL

Peter Crimi

Avco Systems Division

Prepared for:

Army Research Office-Durham

April 1974

DISTRIBUTED BY:

NTIS

**National Technical Information Service
U. S. DEPARTMENT OF COMMERCE
5285 Port Royal Road, Springfield Va. 22151**

Unclassified

Security Classification

AD 779549

DOCUMENT CONTROL DATA - R & D		
<i>(Security classification of title, body of abstract and indexing annotation must be entered when the overall report is classified)</i>		
1. ORIGINATING ACTIVITY (Corporate author) Avco Government Products Group Avco Systems Division 201 Lowell Street Wilmington, Mass. 01887		2a. REPORT SECURITY CLASSIFICATION Unclassified
		2b. GROUP NA
3. REPORT TITLE THEORETICAL STUDY OF DYNAMIC STALL		
4. DESCRIPTIVE NOTES (Type of report and inclusive dates) Final Report		
5. AUTHOR(S) (First name, middle initial, last name) Peter Crimi		
6. REPORT DATE April 1974	7a. TOTAL NO. OF PAGES 46	7b. NO. OF REFS 26
8a. CONTRACT OR GRANT NO. DAHC04-71-C-0017	8c. ORIGINATOR'S REPORT NUMBER(S) AVSD-0119-74-RR	
8b. PROJECT NO.	8d. OTHER REPORT NO(S) (Any other numbers that may be assigned this report)	
9.		
10. DISTRIBUTION STATEMENT Approved for public release; distribution unlimited		
11. SUPPLEMENTARY NOTES	12. SPONSORING MILITARY ACTIVITY U, S. Army Research Office - Durham Box CM, Duke Station Durham, North Carolina 27706	
13. ABSTRACT An analysis of unsteady trailing-edge stall of a two-dimensional airfoil was carried out, the objectives being to develop tools for analysis of the general dynamic stall problem and to gain further understanding of the underlying mechanisms of the unsteady stall process. The problem was first formulated to take direct account of the interactions of the viscous and inviscid flows, but an acceptable matching of the potential-flow and viscous-flow solutions could not be obtained. A different approach was then taken, whereby the effects of the viscous flow were introduced through imposition of a boundary condition on pressure along a surface in the separated flow region. A satisfactory solution was obtained for steady separated flow, but numerical difficulties prevented a solution in the unsteady case. While it would appear possible to obtain a solution to the general nonlinear problem by further development of the second approach, it is recommended, instead, that a linearized formulation be systematically refined to account for nonlinear effects.		

DD FORM 1473

REPLACES DD FORM 1473, 1 JAN 60, WHICH IS OBSOLETE FOR ARMY USE.

Unclassified
Security Classification

Reproduced by
NATIONAL TECHNICAL
INFORMATION SERVICE
U S Department of Commerce
Springfield VA 22151

Unclassified
Security Classification

KEY WORDS	LINK A		LINK B		LINK C	
	ROLE	WT	ROLE	WT	ROLE	WT
Dynamic stall						
Unsteady aerodynamics						
Rotary wings						

ia

Unclassified
Security Classification

THEORETICAL STUDY OF DYNAMIC STALL
FINAL REPORT

by
Peter Crimi

April 1974
AVSD-0119-74-RR

Prepared for
U. S. ARMY RESEARCH OFFICE - DURHAM

Contract No. DAHC04-71-C-0017

Prepared by
AVCO GOVERNMENT PRODUCTS GROUP
Avco Systems Division
201 Lowell Street
Wilmington, Massachusetts 01887

APPROVED FOR PUBLIC RELEASE:
DISTRIBUTION UNLIMITED

ib

THE FINDINGS IN THIS REPORT ARE NOT TO BE
CONSTRUED AS AN OFFICIAL DEPARTMENT OF
THE ARMY POSITION, UNLESS SO DESIGNATED
BY OTHER AUTHORIZED DOCUMENTS.

ie

FOREWORD

This report was prepared by Avco Systems Division, Wilmington, Massachusetts, for the U. S. Army Research Office, Durham, North Carolina, in accordance with the requirements of Contract No. DAHC04-71-C-0017.

Dr. Peter Crimi was Principal Investigator for the reported study. Substantive contributions were made by Dr. Barry L. Reeves in the development of the viscous-flow representations.

Technical monitorship was provided by Mr. James J. Murry and Dr. Robert E. Singleton of the U. S. Army Research Office - Durham.

CONTENTS

	<u>Page</u>
SUMMARY	iv
1.0 INTRODUCTION	1
2.0 STALL MECHANISMS -- PROBLEM DEFINITION	4
3.0 FLOW ELEMENT REPRESENTATIONS	8
3.1 POTENTIAL FLOW	8
3.2 BOUNDARY LAYER	13
3.3 SEPARATED FLOW REGION	13
4.0 ANALYSIS PROCEDURES	23
5.0 DISCUSSION OF RESULTS	25
6.0 REFERENCES	33
APPENDIX	36

1.0 INTRODUCTION

Helicopter operation at high forward speed requires that the retreating blade of the rotor achieve a high lift coefficient. As a result, under conditions of maximum performance, the flow periodically separates from and reattaches to portions of each blade, giving rise to severe control loads, increased vibration levels and, at times, a dangerously large response in the fundamental blade torsional mode (Ref. 1). An understanding of the mechanisms of stall onset in unsteady flow and the effect of blade section parameters and flight conditions on dynamic stall and the associated loading would clearly benefit future designs. The helicopter stall problem provided the primary motivation for the study reported here.

Dynamic stall is involved in continuing problems in other areas as well. Notable examples are rotating stall in axial-flow compressors (Ref. 2) and stall flutter of propellers and compressor blading (Ref. 3).

Early experimental studies of unsteady stall, such as those reported in References 4 and 5, were concerned primarily with the stall flutter problem. From this work, the stall flutter mechanism of negative damping, or moment variation to extract energy from the flow, was deduced. More recently extensive tests on two-dimensional airfoils sinusoidally pitching or plunging through stall were carried out (Ref. 6) which make evident the complexity of the unsteady stall process. Both lift overshoot, or lift in excess of the maximum static value, and unstable moment variation were found to be strong functions of frequency, amplitude, mean incidence and Mach number.

Other tests, of more limited scope but employing specialized instrumentation and flow visualization techniques, have revealed a number of important aspects of the problem. The formation of a leading-edge bubble, normally associated with airfoils subject to leading-edge stall, was detected in tests on model rotor blades (Refs. 7 and 8). Details of the stall onset process during leading edge stall, wherein a region of highly rotational flow forms at the leading edge and grows progressively from the leading to the trailing edge, was described in Reference 1 and was later observed in tests on a model rotor blade (Ref. 9) and on a two-dimensional airfoil (Ref. 10).

Analytical studies of various aspects of the stall problem as it relates to helicopter rotor blades have been carried out. Patay (Ref. 11) analyzed the unsteady boundary layer on a pitching Joukowski airfoil, and concluded that the flow in the boundary layer is essentially quasi-steady for dimensionless pitch rate $\theta b/U$ as large as .05, where b is semichord and U is

free stream speed. Analyses of the unsteady laminar boundary layer on a rotating blade (Ref. 8) similarly showed that the chordwise pressure gradient dominates over both unsteady and rotational effects. The unsteady load on an oscillating stalled airfoil, for prescribed separation point location, was derived by Woods (Ref. 12), using classical unsteady thin-airfoil theory as a basis.

A number of analyses of unsteady stall of two-dimensional airfoils and rotors have been performed with viscous effects taken into account empirically. Ham (Ref. 13) analyzed a two-dimensional model consisting of discrete vortices shed from both the leading and trailing edges. Ericsson and Reding (Ref. 14) employed a quasi-steady approach which uses measured static airfoil characteristics. Carta and Niebanck (Ref. 15) utilized data from tests of two-dimensional oscillating airfoils and energy considerations to analyze stall flutter of a rotor blade. Rotor control loads due to stall are predicted by Tarzanin (Ref. 16) using an empirical model, again derived from data taken on oscillating airfoils, from which instantaneous loading during stall is computed. These methods generally yield good correlations with test data.

In the analyses of dynamic stall reported in Refs. 17 and 18, viscous-inviscid interactions are taken into account analytically, in order to gain better insight into the underlying mechanisms of the unsteady stall process. A number of approximations were employed in the representations of the individual flow elements, in order to make the problem tractable, which caused rather large discrepancies between the theory and test results. Nonetheless, quite good qualitative agreement with measured loading was obtained, with both lift overshoot and accompanying large nose-down moment in evidence in the computed results for transient pitching through stall.

The study reported here was undertaken as a complement to those of Refs. 17 and 18. A specific type of unsteady stall, namely trailing-edge stall, which has clearly defined flow elements and stall mechanisms, was analyzed in detail. The objectives were to obtain a measure of what approximations can reasonably be employed in analyzing the more general problem, by providing a rigorous solution for comparison, and, hopefully, to gain further knowledge of the unsteady stall process.

Unfortunately, the primary objectives of the study were not realized. Viscous and inviscid solutions could not be matched to an acceptable degree, using either of two different approaches to the problem. Some positive results were obtained. The method used to compute the unsteady potential flow, which is based primarily on the method developed by Giesing (Ref. 19) but with a continuous wake representation, proved to be both readily

implemented and accurate. Also, a quite general formulation of the unsteady turbulent mixing and reattachment processes has been generated.

The specific problem analyzed is delineated in the next section. The formulations of the individual flow elements are then presented, and the two different methods used to account for viscous-inviscid interaction are outlined. The results obtained and the probable causes for the failure to obtain solutions in the general case are discussed in the last section.

2.0 STALL MECHANISMS -- PROBLEM DEFINITION

The specific system analyzed consists of an airfoil of infinite span subjected to an incompressible, uniform free stream. The airfoil incidence relative to the free stream is varying due to pitching motion about some point along the chord, translational or plunging motion, and changes in the magnitude of the free stream. When the flow is attached, a thin boundary layer of adhering fluid surrounds the airfoil, outside of which is a continuous, irrotational flow. Because the load on the airfoil is changing with time, implying a rate of change of circulation about the airfoil, a thin vortical wake is shed from the trailing edge (Point T in Figure 1a), to conserve total circulation. This distribution of vorticity is convected downstream at nearly the free-stream velocity.

As the effective incidence increases, an adverse pressure gradient builds up until, by one of several mechanisms to be discussed subsequently, the flow separates from some point S on the airfoil surface, leaving a zone of more or less stagnant fluid attached to the airfoil, as indicated in Figure 1b. It is assumed, based on what occurs in steady flow, that the trapped-air region consists of a zone which is at nearly a constant pressure, somewhat below free-stream static pressure, out to point R, downstream of which is a region of mixing with the free stream and pressure recovery. The load on the airfoil is again changing with time, so a sheet of vortical fluid is convected from the trailing edge. Since the point S is also a terminus of the wake, vorticity is shed from that point as well when the airfoil is stalled.

The mechanism of stall onset is extremely complex and depends on many parameters, including Reynolds number, leading-edge radius, airfoil thickness, camber, sweep, Mach number, and the pressures imposed by unsteady motion. It is generally accepted, though, that a given airfoil stalls in one of three ways, as first discussed in Ref. 20. The three types of stall are termed, respectively, trailing-edge stall, leading-edge stall and thin-airfoil stall.

Trailing-edge stall is the most easily identified of the three types, being due to the separation of the turbulent boundary layer near the trailing edge. Increasing incidence moves the point of separation progressively forward along the airfoil, resulting in a gradual decrease in lift and increase in drag, as indicated in Figure 2a. This type of stall generally occurs on relatively thick airfoils at high Reynolds numbers.

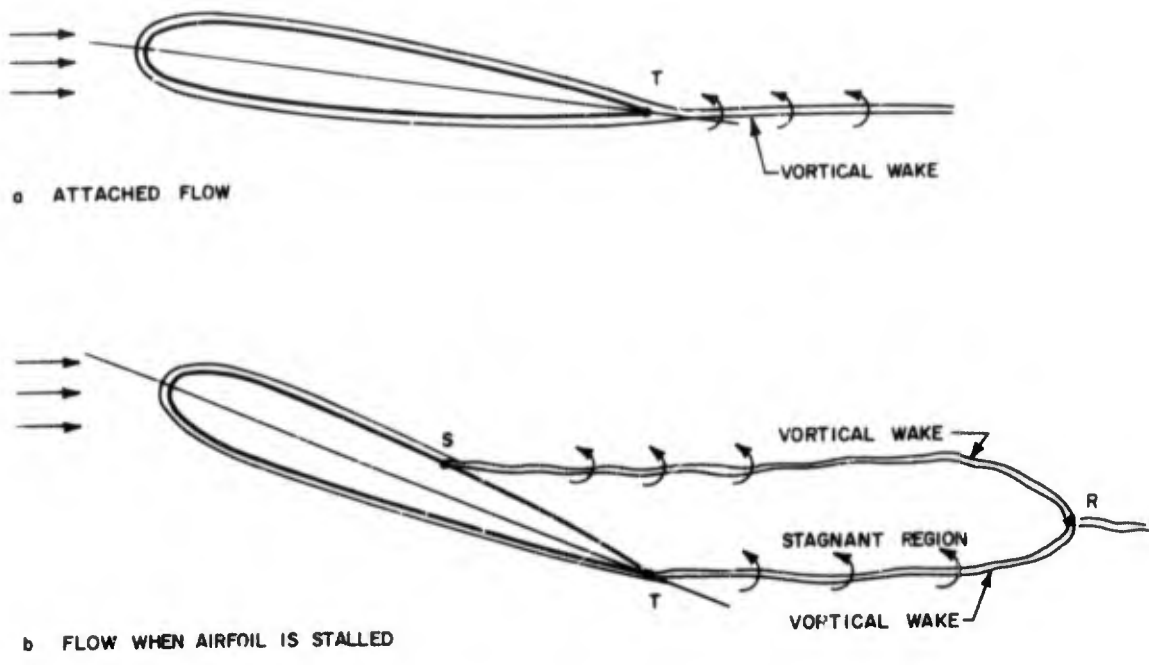
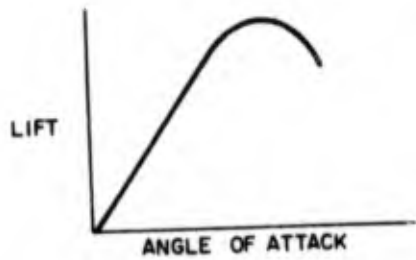


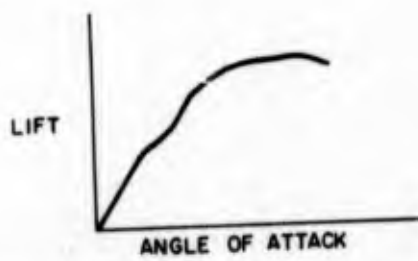
Figure 1 FLOW ELEMENTS DURING DYNAMIC STALL



a TRAILING-EDGE STALL



b LEADING-EDGE STALL



c THIN-AIRFOIL STALL

Figure 2 THE THREE TYPES OF AIRFOIL STALL

Leading-edge stall is related to the formation of a small separation bubble near the leading edge. At a fairly low incidence, laminar separation occurs near the point of minimum pressure at the leading edge. The flow reattaches a short distance downstream of the separation point due to transition from laminar to turbulent flow in the free shear layer with subsequent turbulent mixing and reattachment. As angle of attack increases, the bubble is seen to move closer to the leading edge, grow slightly shorter and somewhat thicker. The bubble has almost no effect on integrated loads, since it is never more than a few percent of chord in length. At some angle of attack, the bubble bursts and the flow separates from the entire upper surface of the airfoil, resulting in a sudden loss in lift, as indicated in Figure 2b. The precise reason for the bursting of the laminar bubble has been the subject of considerable controversy. There have been correlations attempted with bubble length and with boundary-layer momentum thickness at the point of laminar separation, with little success. There is a strong indication, though, that there is some maximum amount of pressure recovery which can occur in the turbulent mixing zone and still allow reattachment, and at some incidence the required recovery exceeds this maximum, causing sudden separation. A thorough and well-ordered discussion of the various theories and evidence related to leading-edge stall is given in Ref. 21.

Thin-airfoil stall is characterized by the appearance of a laminar bubble springing from the leading edge at a relatively low incidence. Unlike the bubble formed prior to leading-edge stall, its point of separation remains fixed with increasing incidence while the bubble grows progressively larger. The processes of bubble formation and reattachment are not well understood (Ref. 21). The resulting lift curve is as sketched in Figure 2c.

Clearly, a rigorous modelling of the flow processes involved in airfoil stall, even under steady conditions, would be extremely difficult. The problem is compounded in the unsteady case by the present uncertainties concerning the mechanisms of stall onset and subsequent development of the trapped-air region. However, if consideration is limited to trailing-edge stall, the primary flow elements and the stall onset process can be clearly defined. In light of the previously stated objectives, then, this study was concerned with the particular case of trailing-edge stall, and hence with the interactions of the boundary layer, the potential flow, and the turbulent mixing and reattachment regions, with the progression of stall determined by the location of the separation point of the turbulent boundary layer.

3.0 FLOW ELEMENT REPRESENTATIONS

3.1 POTENTIAL FLOW

While two different approaches to the interaction problem were attempted, the same basic potential-flow model was used for both, the formulations of the boundary conditions being basically of the same form, i. e., a flow direction requirement on the wetted surface and a flow magnitude requirement in the region of separated flow. The problem is formulated in terms of coordinates (x, y) fixed to the airfoil, which has unit chord length, as shown in Figure 3. The fluid velocity \underline{q} , relative to an inertial frame, is taken to be the gradient of a potential ϕ . If the airfoil has a translational velocity \underline{V} and angular velocity $\underline{\omega}$, the fluid velocity relative to the airfoil \underline{q}_r , at a point located by vector \underline{r} , is given by

$$\underline{q}_r = \nabla \phi - (\underline{V} + \underline{\omega} \times \underline{r})$$

The boundary condition on the wetted surface is

$$\underline{q}_r \cdot \underline{n} = 0$$

\underline{n} being the unit vector normal to the surface, and in the separated-flow region,

$$\underline{q}_r \cdot \underline{t} = q_v$$

where q_v is a function obtained from the viscous-flow analysis and \underline{t} is the unit vector tangent to the surface.

The pressure coefficient c_p is computed from the following relation, once a solution has been obtained (Ref. 19):

$$c_p = - \frac{1}{U_0^2} \left[q^2 + 2 \frac{\partial \phi}{\partial t} - 2 (\underline{V} + \underline{\omega} \times \underline{r}) \cdot \underline{q} \right]$$

U_0 being the reference speed.

The potential has been formulated in terms of finite elements, using an approach similar to that of Ref. 19. It would not be practical, for this problem, to divide the potential into separate circulatory and noncirculatory parts, so a somewhat more direct procedure was used. The surface on which the boundary conditions are imposed is divided into finite rectilinear elements, N_G in number, with the source strength assumed to be constant

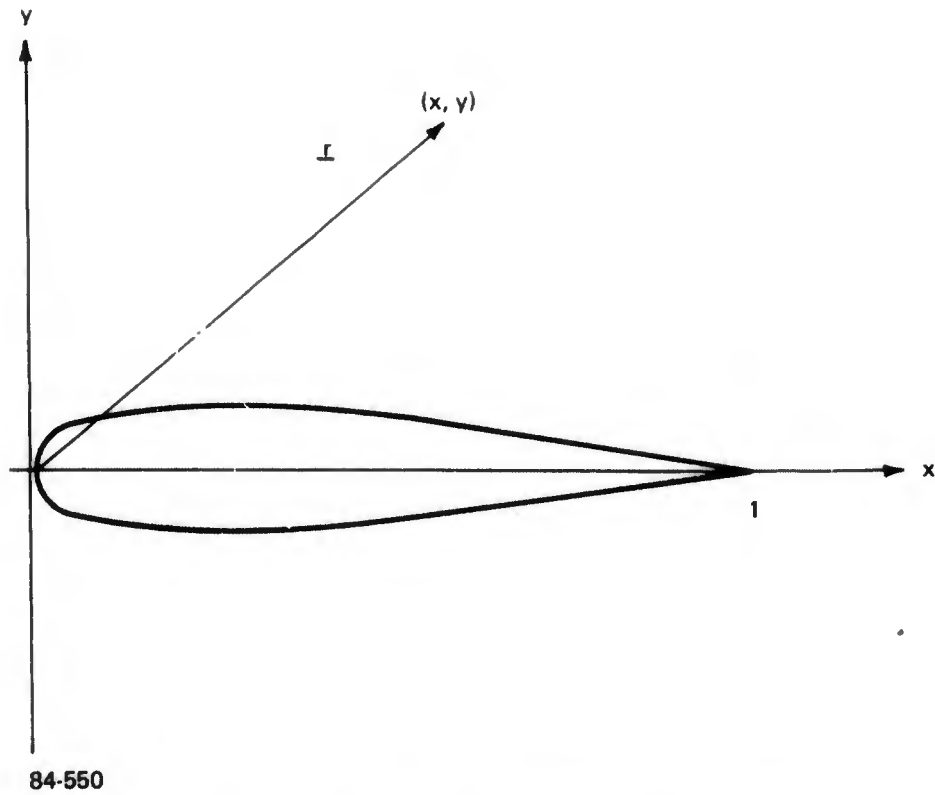


Figure 3 COORDINATE SYSTEM FOR POTENTIAL FLOW

(at a given instant) over each element. Bound vorticity of prescribed analytical form is distributed on the x-axis between the leading and trailing edges. The shed vortex wake is assumed to consist of rectilinear elements with vortex strength varying linearly between end points. Wake displacement is determined by computing the flow at element end points. The bound vorticity strength γ_b is of the following form:

$$\gamma_b = 6x(1-x)\Gamma + x(3x-2)\gamma_1 + x(1-x)(1-2x)\gamma_{s1} + 16x(1-x)[5x(1-x)-1]\gamma_{s2}$$

It can be verified that, with γ_b in this form,

$$\int_0^1 \gamma_b(x, t) dx \equiv \Gamma'(t)$$

where $\Gamma(t)$ is the instantaneous circulation about the airfoil. It should be noted, too, that γ_b has been constructed such that

$$\gamma_b(1, t) = \gamma_1(t)$$

where γ_1 is the wake strength at the trailing edge, insuring continuity of the vortex strength at that point. The terms with coefficients γ_{s1} and γ_{s2} are included only when the airfoil is stalled, being needed to impose conditions of continuity at the separation point. The two added conditions are that the fluid velocity at the first element downstream of the separation point be tangent to the element and that it be equal in magnitude to that at the adjacent element upstream of the separation point. The vortex strength at the trailing edge, being proportional to the time rate of change of Γ , is expressed by the following finite difference approximation:

$$\gamma_1(t) = -\frac{1}{q_{te} \Delta t} [1.5 \Gamma(t) - 2 \Gamma(t - \Delta t) + .5 \Gamma(t - 2 \Delta t)] \quad (1)$$

where q_{te} is the magnitude of q_r at the trailing edge, obtained by linear extrapolation in time.

A solution is obtained at a given instant by imposing the appropriate boundary condition at the midpoint of each of the surface elements, together with flow continuity conditions and solving the resulting set of linear algebraic equations. The specific procedure derives from the expressions for the components u and v of \underline{q}_r at the midpoint of the i th element (coordinates \bar{x}_i, \bar{y}_i) which are:

$$u(\bar{x}_i, \bar{y}_i) = -V_x - \omega \bar{y}_i + \frac{1}{2\pi} \left\{ \sum_{j=1}^{N_\sigma} u_{ij} \sigma_j + u_{\Gamma_i} \Gamma \right. \\ \left. + u_{\gamma_i} \gamma_1 + u_{s1i} \gamma_{s1} + u_{s2i} \gamma_{s2} \right. \\ \left. + \sum_{k=1}^{N_w} u_{wik} \right\} \quad (2)$$

$$v(\bar{x}_i, \bar{y}_i) = -V_y - (\bar{x}_i - x_p) \omega + \frac{1}{2\pi} \left\{ \sum_{j=1}^N v_{ij} \sigma_j \right. \\ \left. + v_{\Gamma_i} \Gamma + v_{\gamma_i} \gamma_1 + v_{s1i} \gamma_{s1} + v_{s2i} \gamma_{s2} \right. \\ \left. + \sum_{k=1}^{N_w} v_{wik} \right\} \quad (3)$$

where V_x and V_y are the components of \underline{V} and x_p is the pitch-axis location. The various functions appearing in Eqs. (2) and (3) are defined in the Appendix. The unknowns appearing explicitly in Eqs. (2) and (3) are the source strengths σ_j , the circulation Γ and the added bound vortex contributions γ_{s1} and γ_{s2} . From Eq. (1) it is seen that γ_1 depends on $\Gamma(t)$. The terms u_{wik} and v_{wik} are the contributions of wake vortex element k (element 1 is attached to the trailing edge) to the flow at element i ; they depend linearly on the wake strength at the end points of that element, γ_k and γ_{k+1} . Thus, u_{wi1} and v_{wi1} contain terms multiplying γ_1 , and hence $\Gamma(t)$.

In the general case of separated flow, there are $N_{\sigma} + 3$ unknowns. Imposition of the boundary conditions at the midpoints of the surface elements yields N_{σ} linear algebraic equations. The Kutta condition and the two continuity conditions at the separation point provide the other three relations needed. In the formulation of those equations, all the various terms multiplying $\Gamma(t)$ are combined into a single matrix element. The equations are solved by successive elimination of unknowns.

In the course of the study, it was thought that the source of the difficulty in obtaining a match between inviscid and viscous flow solutions might be the formulation of the Kutta condition, so two different forms were used. One of these required that the magnitude of the fluid velocity on the upper and lower elements at the trailing edge be equal, and the other required that v be zero at the point on the x -axis between the midpoints of those two elements. Both formulations give satisfactory results for attached flow.

Once a solution is obtained, the pressure coefficient is computed from the following relation:

$$c_p(\bar{x}_i, \bar{y}_i) = \frac{1}{U_0^2} \left\{ \left[U - \omega \bar{y}_i \right]^2 + \left[V + \omega (\bar{x}_i - x_p) \right]^2 - u^2(\bar{x}_i, \bar{y}_i) - v^2(\bar{x}_i, \bar{y}_i) - 2 \phi(\bar{x}_i, \bar{y}_i) \right\}$$

where U_0 is reference speed and, with second-order differences approximating time derivatives,

$$2\pi \phi = \frac{1}{\Delta t} \sum_{j=1}^{N_{\sigma}} \phi_{ij} \left[1.5 \sigma_j(t) - 2 \sigma_j(t - \Delta t) + .5 \sigma_j(t - 2 \Delta t) \right] - q_{te} \phi_{\Gamma_i} \gamma_1 + \frac{\phi \gamma_1}{\Delta t} \left[1.5 \gamma_1 - 2 \gamma_2 + .5 \gamma_3 \right] + \frac{1}{\Delta t} \sum_{y=1}^2 \phi \gamma_{s_y} \left[1.5 \gamma_{s_y}(t) - 2 \gamma_{s_y}(t - \Delta t) + .5 \gamma_{s_y}(t - 2 \Delta t) \right] - \sum_{k=1}^{N_w} \left[u(\bar{x}_k, \bar{y}_k) u_{wik} + v(\bar{x}_k, \bar{y}_k) v_{wik} \right]$$

The functions ϕ_{ij} , etc., are defined in the Appendix. Coordinates (\bar{x}_k, \bar{y}_k) locate the midpoint of the k^{th} wake element. Force and moment coefficients are obtained by direct integration of c_p .

3.2 BOUNDARY LAYER

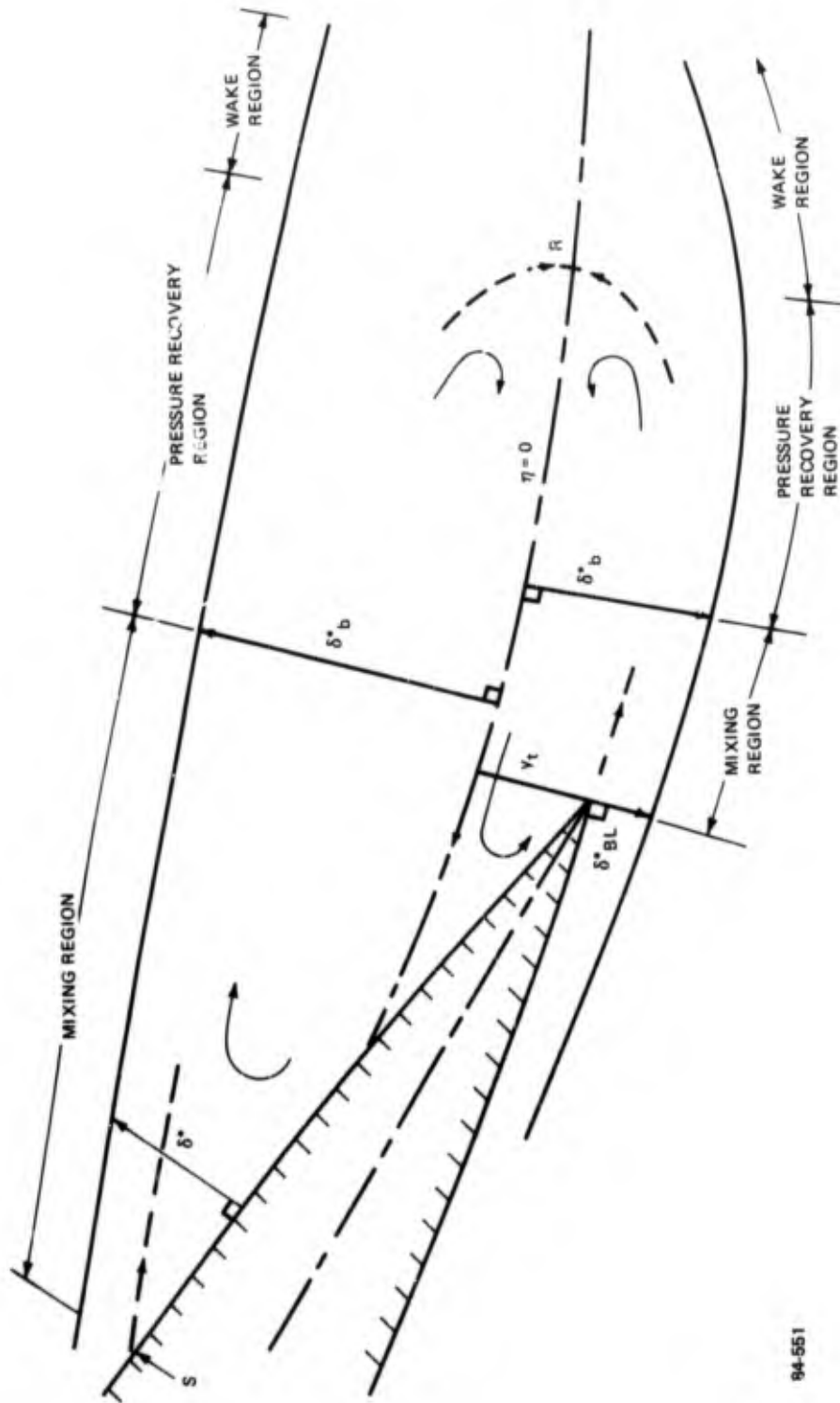
The boundary layer analysis concerns the laminar boundary layer extending from the forward stagnation point on the airfoil over the leading edge, and the turbulent boundary layer which forms downstream of the transition point or downstream of the leading edge bubble, if laminar separation precedes transition.

Both the laminar and the turbulent boundary layers are analyzed by the method of finite differences for unsteady flow. The detailed formulations used are given in Ref. 17. The Smith-Cebeci eddy-viscosity model is employed to represent turbulent shear. The method uses variable step size in both the streamwise and normal directions, the error in each finite-difference approximation being of the order of the square of step size. The solution at each streamwise step is obtained by iteration, using wall shear as the convergence criterion, with nonlinear terms estimated from extrapolation formulas during the first iteration. In order to minimize computer storage requirements associated with evaluation of time derivatives, provision is made for expanding the mesh in the normal direction, keeping the number of mesh points constant, when the boundary layer thickness exceeds a prescribed limit.

The initial profile for the laminar boundary layer is taken from the Heimenz stagnation point solution (Ref. 22). It was assumed, for this study, that transition occurs at the point of minimum pressure near the leading edge, precluding laminar separation and subsequent formation of a leading edge bubble. The analysis proceeds continuously from the laminar to the turbulent boundary layer by introducing turbulent shear gradually over a small but finite distance. The separation point of the turbulent boundary layer was taken to be the point of vanishing wall shear even though the two are not generally coincident in unsteady flow (Ref. 23). There is some evidence, however, as reported in Ref. 18, that this approximation is a reasonable one in most circumstances of practical interest.

3.3 SEPARATED FLOW REGION

The analysis of the separated flow region assumes that the flow has the same basic components as are found in steady separated flows. As indicated in Figure 4, there are two layers of turbulent shear flow, one of which originates at the separation point S and the other from the lower



94-551

Figure 4 ELEMENTS OF THE SEPARATED FLOW

surface boundary layer at the trailing edge. Both layers have a mixing region, which is at nearly constant pressure in steady flow, and a pressure-recovery or compression region, terminated at a common stagnation point R. A wake region extends downstream of point R.

The formulations were developed as a generalization of the ones employed in Ref. 17, by including time derivatives in the controlling differential equations and solving those equations numerically rather than by approximate analytical means. As in Ref. 17, it is assumed that the flow has a wake-like character, and that the equilibrium wall layer usually present in attached turbulent flows can be ignored. Also, the wall shear stress is assumed to be negligible compared to the properly normalized rate of change of momentum thickness and the streamwise pressure gradient.

The specific formulations employed are developed as follows. With negligible wall shear, the momentum integral and first moment equations for the turbulent shear layer can be written in the form

$$\frac{\partial \theta}{\partial \xi} + \frac{\theta}{u_e} \frac{\partial u_e}{\partial \xi} \left(2 + \frac{\delta^*}{\theta}\right) + \frac{1}{u_e} \frac{\partial \delta^*}{\partial t} + \frac{\delta^*}{u_e^2} \frac{\partial u_e}{\partial t} = 0 \quad (4)$$

$$\frac{\partial \theta^*}{\partial \xi} + \frac{3 \theta^*}{u_e} \frac{\partial u_e}{\partial \xi} + \frac{1}{u_e} \frac{\partial \delta^*}{\partial t} + \frac{1}{u_e} \frac{\partial \theta}{\partial t} + \frac{\theta}{u_e^3} \frac{\partial u_e^2}{\partial t} = D \quad (5)$$

where u_e is the magnitude of the fluid velocity in the external inviscid flow, ξ is the coordinate in the streamwise direction, and

$$\delta^* = \int_0^{\delta} \left(1 - \frac{u_v}{u_e}\right) d\eta \quad \theta = \int_0^{\delta} \frac{u_v}{u_e} \left(1 - \frac{u_v}{u_e}\right) d\eta$$

$$\theta^* = \int_0^{\delta} \frac{u_v}{u_e} \left(1 - \frac{u_v^2}{u_e^2}\right) d\eta \quad D = 2 \int_0^{\delta} \frac{\tau}{\rho u_e^2} \frac{\partial u_v}{\partial \eta} d\eta$$

in which η is the coordinate normal to ξ , δ is layer thickness, u_v is the magnitude of the fluid velocity and τ is the shear stress.

The assumption that the flow is wake-like leads to the selection of a set of velocity profile parameters which are assumed to be functions of a single parameter a , where

$$a = \frac{\eta (u_v = 0)}{\delta}$$

Those parameters are denoted H , J , \bar{R} and K_θ , and are defined by

$$\begin{aligned} H &\equiv \theta/\delta^*, & J &\equiv \theta^*/\delta^*, \\ D &= K_\theta H \bar{R}, & \bar{R} &\equiv \frac{2\delta^*}{u_e^3} \int_0^\delta \left(\frac{\epsilon}{\epsilon_m}\right) \left(\frac{\partial u_v}{\partial \eta}\right)^2 d\eta \end{aligned}$$

where ϵ is eddy viscosity and ϵ_m the maximum of ϵ . Expressed in terms of these parameters, Eqs. (4) and (5) become

$$\begin{aligned} (1 - H) \frac{\partial u_e}{\partial \xi} &= u_e \left(\frac{H}{J} \frac{dJ}{dH} - 1 \right) \frac{\partial H}{\partial \xi} + \frac{H}{J} \frac{\partial H}{\partial t} + \frac{1}{\delta^*} \left[(1 + H) \frac{H}{J} - 1 \right] \frac{\partial \delta^*}{\partial t} \\ &+ \frac{1}{u_e} \left(2 \frac{H^2}{J} - 1 \right) \frac{\partial u_e}{\partial t} - \frac{K_\theta H^2 \bar{R} u_e}{J \delta^*} \end{aligned} \quad (6)$$

$$\begin{aligned} (1 - H) \frac{\partial \delta^*}{\partial \xi} &= \delta^* \left(3 - \lambda \frac{dJ}{dH} \right) \frac{\partial H}{\partial \xi} - \frac{\lambda \delta^*}{u_e} \frac{\partial H}{\partial t} + \frac{1}{u_e} \left[3 - \lambda (1 + H) \right] \frac{\partial \delta^*}{\partial t} \\ &+ \frac{\delta^*}{u_e^2} \left(3 - 2 \lambda H \right) \frac{\partial u_e}{\partial t} + \lambda K_\theta H \bar{R} \end{aligned} \quad (7)$$

where $\lambda = (2H + 1)/J$

For the mixing and reattachment regions, the functional dependence of the profile parameters on a were taken from Ref. 24, which gives the solution for a laminar, and hence constant-viscosity, shear flow. Specifically, these parameters are computed from

$$H = \sum_{k=0}^7 h_k a^k,$$

$$J = \sum_{k=0}^5 j_k a^k$$

$$\frac{dJ}{dH} = \sum_{k=0}^5 d_k a^k$$

$$\bar{R} = \sum_{k=0}^6 r_k a^k$$

$$K_\theta = .05 - .030769H(a)$$

The coefficients of the above polynomials are listed in Table I.

Similarly, downstream of the recovery point, the laminar wake solution of Ref. 25 was used to provide the functional dependence of the profile parameters. The expressions used are:

$$H = .429 + .59631 a, \quad J = .654 + .97446 a + .35316 a^2,$$

$$dJ/dH = 1.63415 + 1.18448 a, \quad K_\theta = .0368,$$

$$\bar{R} = .4634 - 1.2668 a + .8797 a^2$$

Equations (6) and (7) are solved for the dependent variables u_e and δ^* by numerical integration, the key assumption being that the parameter a is a universal function of a suitably normalized streamwise coordinate \tilde{x} . Different functions and definitions for \tilde{x} are used for the mixing region and the pressure recovery and wake regions.

In the mixing region, \tilde{x} is defined according to

$$\tilde{x} = (\xi - \xi_s) / \delta_s^*$$

where subscript s denotes the conditions at separation. The variation of a with \tilde{x} is assumed to be that which results in the case of steady flow. With steady flow, Eq. (6) reduces to

$$(\delta_s^* H_s) \left(\frac{dJ}{dH} - \frac{J}{H} \right) \frac{dH}{d\xi} = K_\theta H^2 \bar{R}$$

TABLE I

Polynomial Coefficients

k	h_k	j_k	d_k	r_k
0	.429	.654	1.51233	.463
1	-.43501	-.75002	-.84718	.40126
2	-.74672	.57812	3.35038	2.58307
3	.24826	-9.0153	-13.9779	-12.4697
4	-.74078	18.5434	5.5206	72.4300
5	-18.8515	-10.1803	30.4187	-136.9234
6	67.2597	0.0	0.0	89.9296
7	-54.1810	0.0	0.0	

since, for steady flow in the mixing region, $du_e/d\xi = 0$ and $\delta^* H$ is a constant. Whence

$$d \left(\frac{\xi - \xi_s}{\delta_s^*} \right) = H_s \left(\frac{dJ}{dH} - \frac{J}{H} \right) \frac{dH}{K_\theta H^2 \bar{R}}$$

$$\text{and } \tilde{x} = H_s \int_{H_s}^H \left(\frac{dJ}{dH} - \frac{J}{H} \right) \frac{(dH/da)}{K_\theta H^2 \bar{R}} da$$

Evaluation of the above integral provides the universal function applicable to the mixing region. The result of that integration is shown graphically in Figure 5.

To obtain the universal function for the pressure recovery and wake regions, an exact solution of a supersonic viscous-inviscid interaction was obtained numerically, with shear layer parameters suitably transformed in the solution to remove their dependence on Mach number. The results are shown in Figure 6, where parameter a and the ratio of δ^* to a reference displacement thickness δ_0^* are plotted against the ratio of streamwise coordinate ξ to δ_0^* . In the pressure recovery and wake regions, the normalized streamwise coordinate is defined by

$$\tilde{x} = (\xi - \xi_b) / \delta_b^*$$

where subscript b denotes the conditions at the beginning of the pressure recovery region. Now, with a_b known, the function plotted in Figure 6 provides the values of $(\xi / \delta_0^*)_b$ and $(\delta^* / \delta_0^*)_b$ (the lower branch of the a -curve applies to the pressure recovery region). Then, for a given value of \tilde{x} , a is obtained by computing ξ / δ_0^* from

$$\frac{\xi}{\delta_0^*} = \left(\frac{\delta^*}{\delta_0^*} \right)_b \tilde{x} + \left(\frac{\xi}{\delta_0^*} \right)_b$$

which in turn prescribes a from the variation of a with ξ / δ_0^* given in Figure 6. Integration proceeds continuously from the pressure recovery

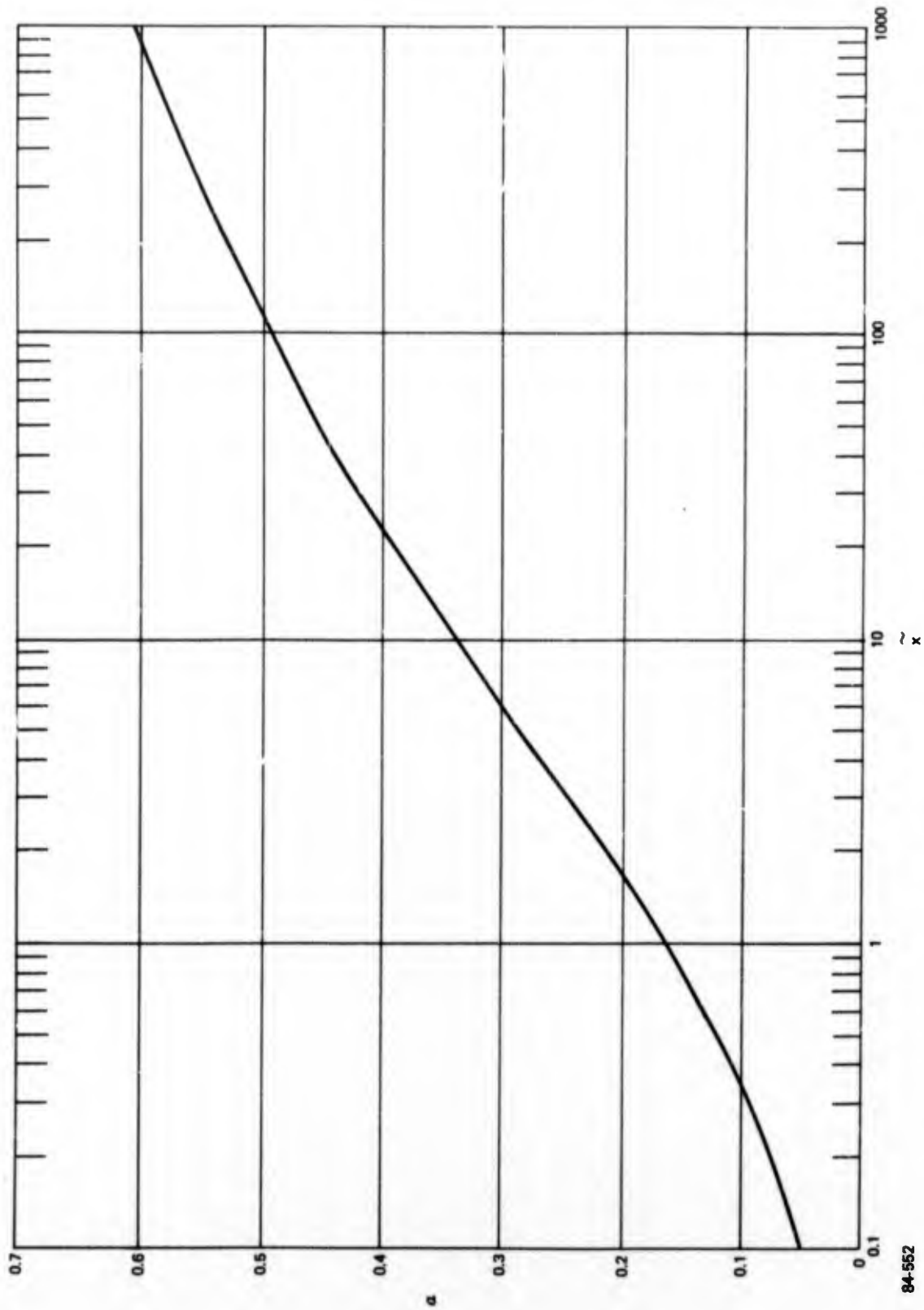


Figure 5 UNIVERSAL FUNCTION FOR MIXING REGION

84-552

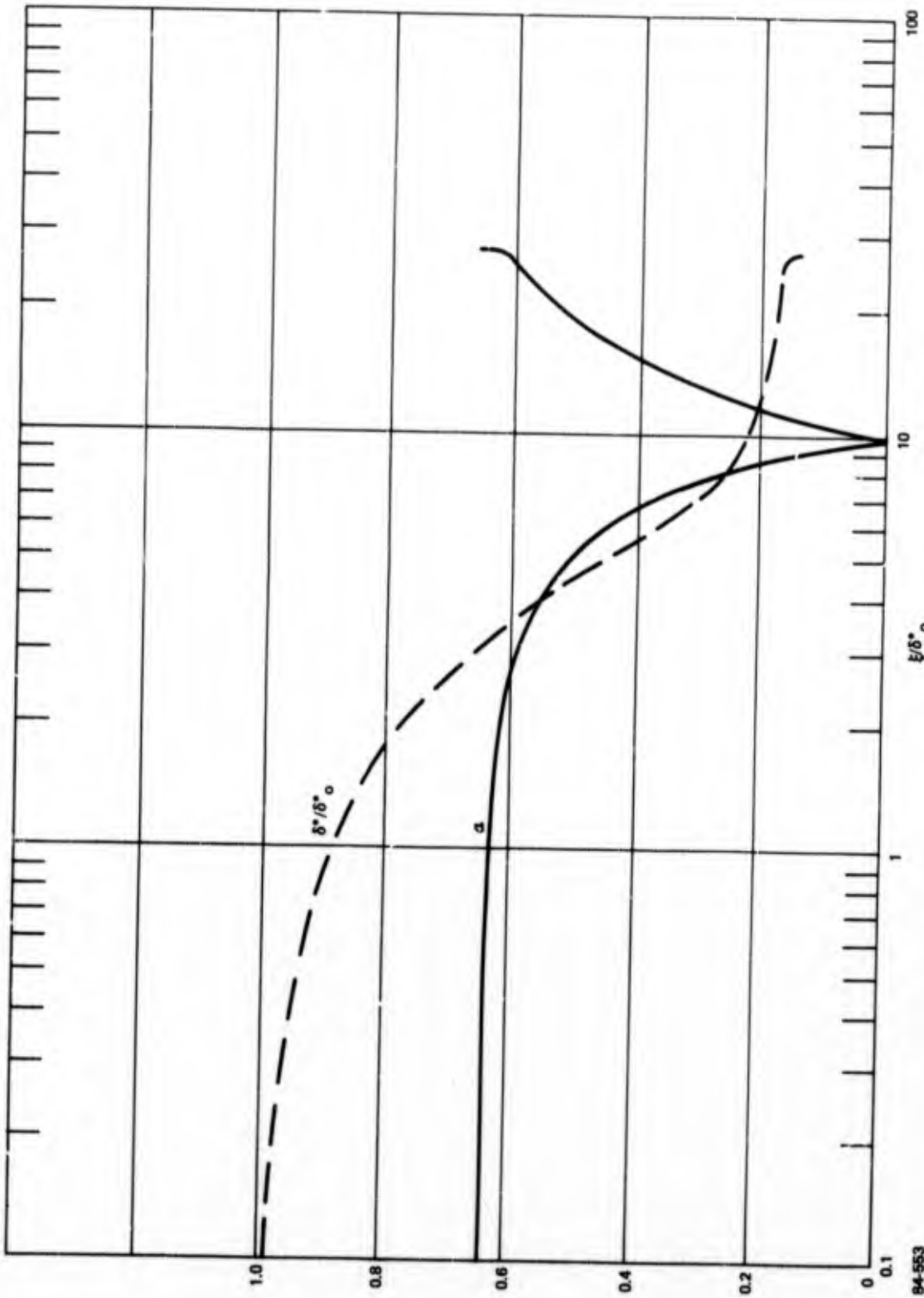


Figure 6 PARAMETERS FOR ANALYSIS OF PRESSURE-RECOVERY AND WAKE REGIONS

region into the wake region, using the upper branch of the a -curve in the wake region. The point where $a = 0$ is the recovery point.

In the two approaches to the viscous-inviscid interaction problem, the formulations of the viscous flow were applied differently. The details of their application are discussed in the next section.

4.0 ANALYSIS PROCEDURES

In the first of the two approaches to the problem, a direct matching of inviscid and viscous flow solutions was attempted. Analyses of the boundary layer and viscous shear layers provided displacement thickness over the airfoil surface and in the separated region, which results were used to define a surface enclosing the airfoil and the separated region. The potential flow determined by the requirement of no flow through that boundary was then obtained, the immediate goal being to match the resulting distribution of pressure external to the separated flow region with the solution for u_e obtained from the shear layer analyses. Location of the separation point was to be obtained by an overall iteration, varying a free parameter in the viscous flow formulation.

Assuming that the airfoil motions are initiated such that the flow is attached, the first step in the direct matching analysis is to compute a potential flow, imposing the appropriate boundary conditions on the airfoil surface. The boundary layer is then analyzed to obtain a first estimate of the separation point location and the displacement thickness and fluid velocity at that point. The upper layer of the separated region is then analyzed by selecting, somewhat arbitrarily, a value for a_b , which is one of the free parameters of the formulation. The integration of Eqs. (6) and (7) determines the variations of u_e and δ^* for the upper layer and the location of the recovery point R. Next, the lower layer is analyzed, starting from the trailing edge, iteratively varying the initial value of the displacement thickness until u_e at the recovery point matches the corresponding value of u_e for the upper layer. The equivalent surface external to the boundary layer and separated region is then defined. This requires specification of the location in terms of airfoil coordinates (x, y) , of the surface $\eta = 0$ dividing the upper and lower shear layers (see Figure 4). The following function was used to prescribe the ordinate of that curve, in terms of the streamwise distance from the trailing edge, $\xi - \xi_t$:

$$y = y_t + A S + \frac{S_e (\sin \alpha - A)}{\delta} \left(\frac{S}{S_e}\right)^\delta$$

where $S = \xi - \xi_t$, δ is a free parameter, α is airfoil angle of attack and S_e is the value of S at the end of the wake region (the wake is arbitrarily truncated several displacement thicknesses downstream of R). The value of A is assigned to make the slope of the boundary of the lower layer continuous at the trailing edge. Note that y_t is the difference between the initial displacement thickness for the lower layer, determined iteratively

to match u_e at R , and the displacement thickness of the lower surface boundary layer at the trailing edge. Upstream of the trailing edge, the surface dividing the two shear layers is taken to be a curve passing through the separation point, tangent to the airfoil, and through the point $y = y_t$ at the trailing edge, matching the slope of the curve downstream of the trailing edge. This formulation leaves two free parameters in defining the separated region, γ and a_b . The intent was to use one of these to match the viscous and inviscid flow solutions and the other to obtain convergence of the separation point location. However, as is discussed in the next section, the variation of u_e as computed from the viscous flow analysis could not be satisfactorily matched with the potential flow solution, so the specific iterative procedures involving γ and a_b were not developed.

The other approach taken is an extension to the nonlinear case of the one used in Ref. 17 to treat the linearized problem. Specifically, the streamwise distribution of pressure as determined by the separated flow analysis is imposed as a boundary condition of the potential flow analysis. The pressure condition is applied on the surface of the airfoil, from the separation point to the trailing edge, and along the surface defined by the shed vortex wake downstream of the trailing edge. There is no need, then, for a direct matching of both flow direction and magnitude; the primary iteration between viscous and inviscid flows is one which locates the separation point. The overall procedure is similar to the one described for direct matching, except that only the upper shear layer need be analyzed. The variation of u_e obtained from that analysis is applied directly as a boundary condition of the potential flow. The main difficulty with this approach in a nonlinear formulation is that the boundary condition on pressure (or more specifically on the magnitude of the fluid velocity) on the airfoil surface is nonlinear, since the direction of the flow is not known a priori in that region. Therefore, it is necessary to perform an iteration to match assumed and computed flow directions along the airfoil surface between the separation point and the trailing edge. This difficulty is not encountered in the linearized problem since to first order the pressure perturbation is simply proportional to the perturbation to the x-component of fluid velocity. This formulation was a definite improvement over the direct matching procedure, since a reasonable potential flow solution could be obtained for steady separated flow. However, as is discussed in the next section, results were unsatisfactory when unsteady effects were included.

5.0 DISCUSSION OF RESULTS

Initial calculations were performed for an unstalled airfoil to verify that the potential flow representation functioned properly. Figure 7 shows the computed chordwise variation of pressure coefficient on a 9% thickness ratio symmetric Joukowski airfoil in steady flow at 8 degrees angle of attack. The corresponding theoretical variation of c_p did not differ from the numerical result sufficiently to distinguish between the two curves using the scale of Figure 7. The loading on an NACA 633-018 airfoil pitching sinusoidally about its quarter-chord point at a reduced frequency (frequency times semichord divided by forward speed) of .1 and a pitch amplitude of .1 rad. was also calculated, assuming steady flow for initial conditions. The airfoil was represented by 42 source elements. Twenty-four time steps were taken per cycle. The variations of lift coefficient and pitch angle θ with time are shown in Figure 8. Note that periodic loading variation is established after only about one cycle of oscillation. The variation of C_l predicted by unsteady thin airfoil theory is also shown in Figure 8 for comparison. The nonlinear effects of thickness are seen to increase the lag in the loading with respect to the pitching motion, as was found in Ref. 19.

In the attempts to obtain a solution for separated flow by direct matching of viscous and inviscid flows, only the steady problem was considered, it being necessary to establish the method for that case before attempting the more general one. All calculations were performed for an NACA 633-018 airfoil at a chordal Reynolds number of 5.8×10^6 .

The procedure described in Section 4 was in fact evolved from a series of different ones formed by successive modifications of an original, considerably more simple procedure. The modifications primarily concerned the prescription of the location of the surface dividing the upper and lower shear layers to obtain a physically realistic boundary of the separated flow region. The formulation given in Section 4 did provide a fairly good result in that respect. However, neither of the two free parameters (γ and a_b), when varied over the entire range permitted by mathematical limitations, was capable of producing an acceptable matching of inviscid and viscous flow solutions. One of the better results is shown in Figures 9, 10, and 11, where the magnitudes of the fluid velocity are compared and the boundaries of the inviscid flow are plotted for $\gamma = 2$ and $a_b = .41$. The airfoil was at an angle of attack of .25 rad and the separation point was at $x = .75$. The potential solution is seen to take large excursions in the vicinity of the trailing edge, and the potential flow and viscous flow solutions differ by

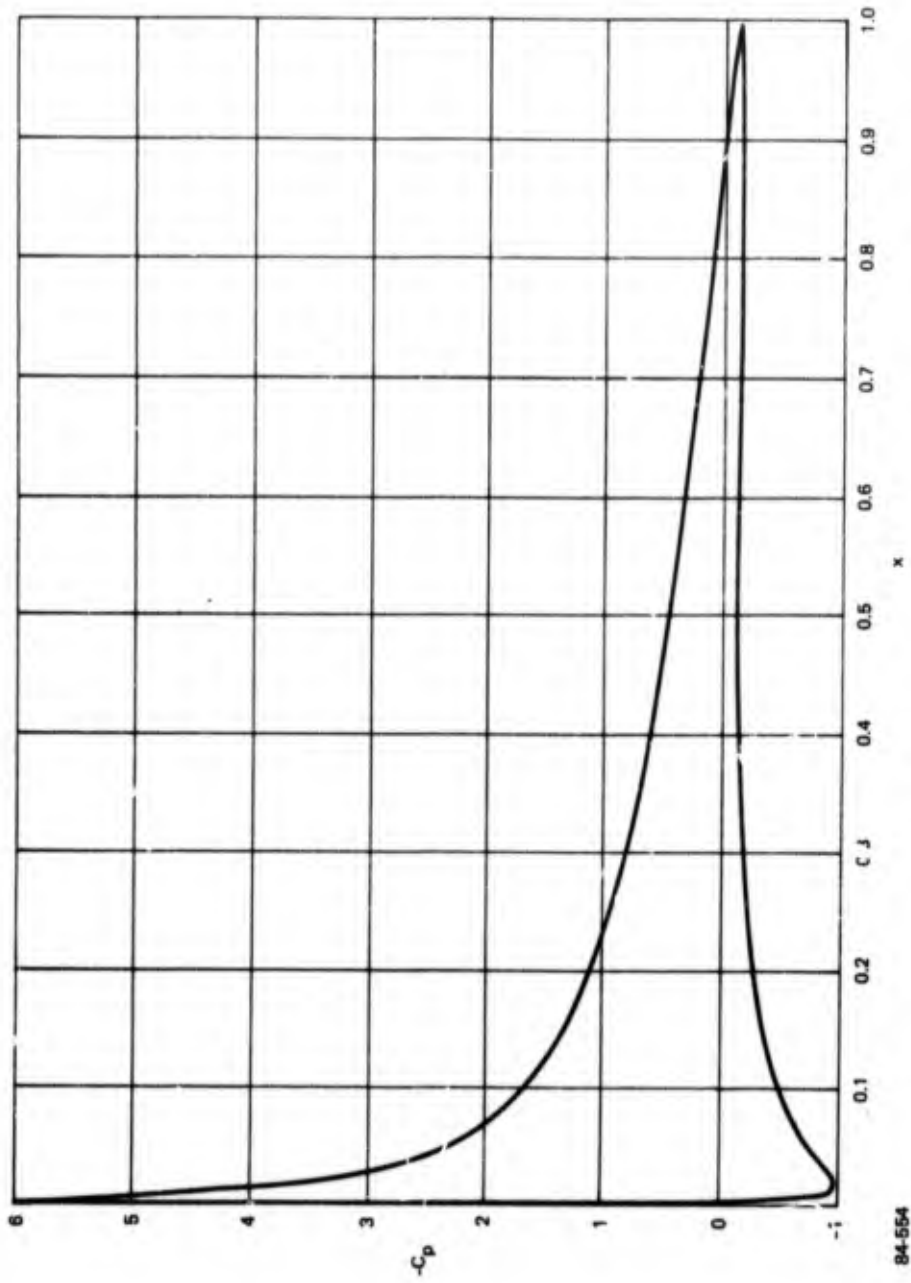


Figure 7 COMPUTED PRESSURE DISTRIBUTION ON A 9 PERCENT JOUKOWSKI AIRFOIL AT 8 DEGREE ANGLE OF ATTACK

84-554

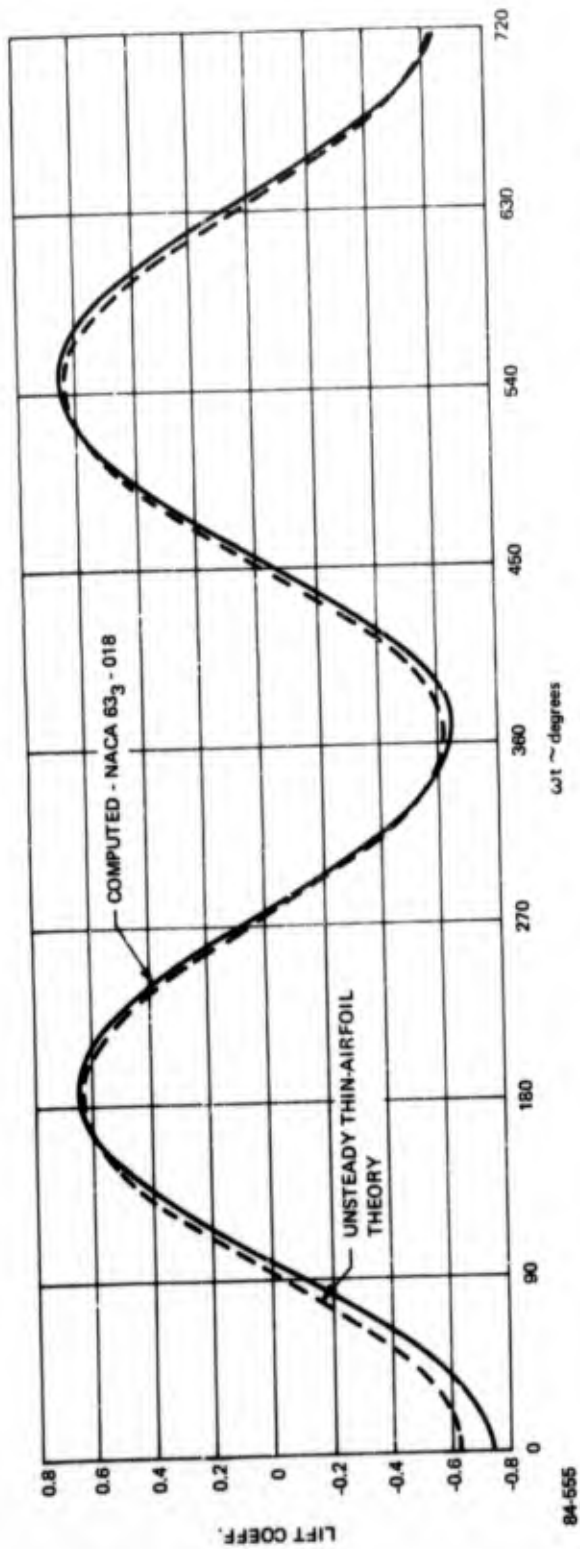
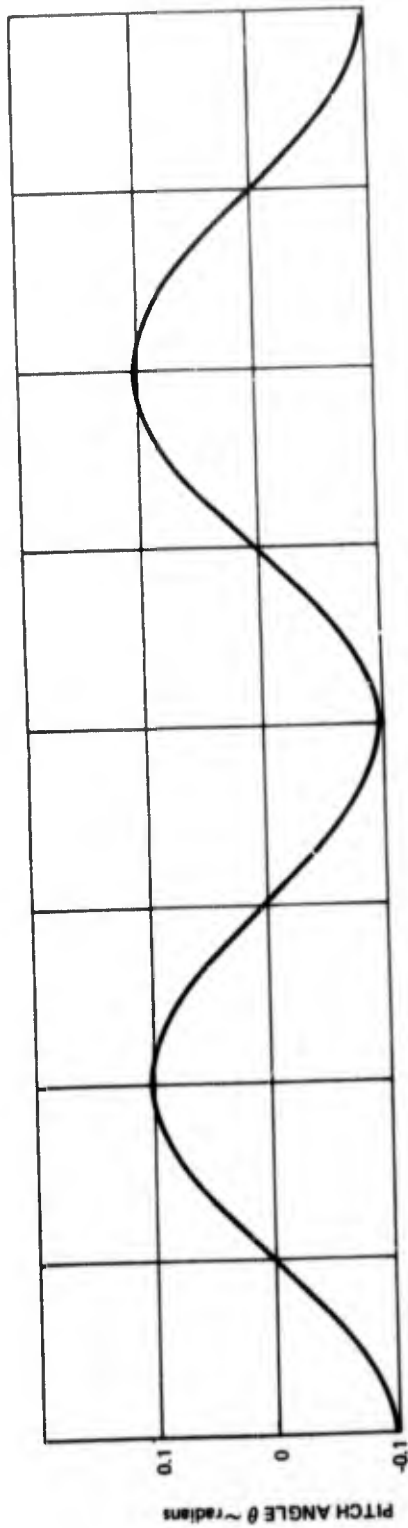
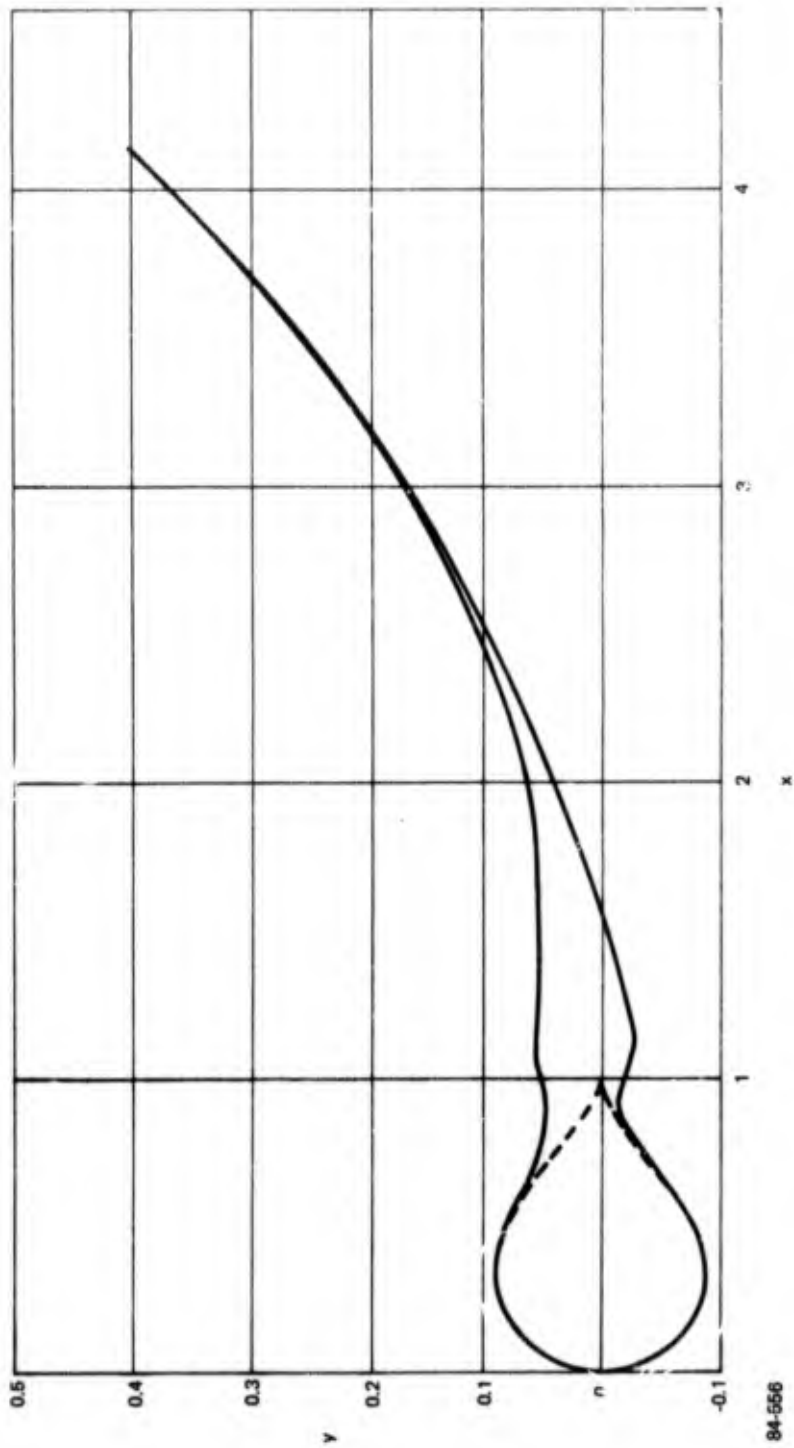
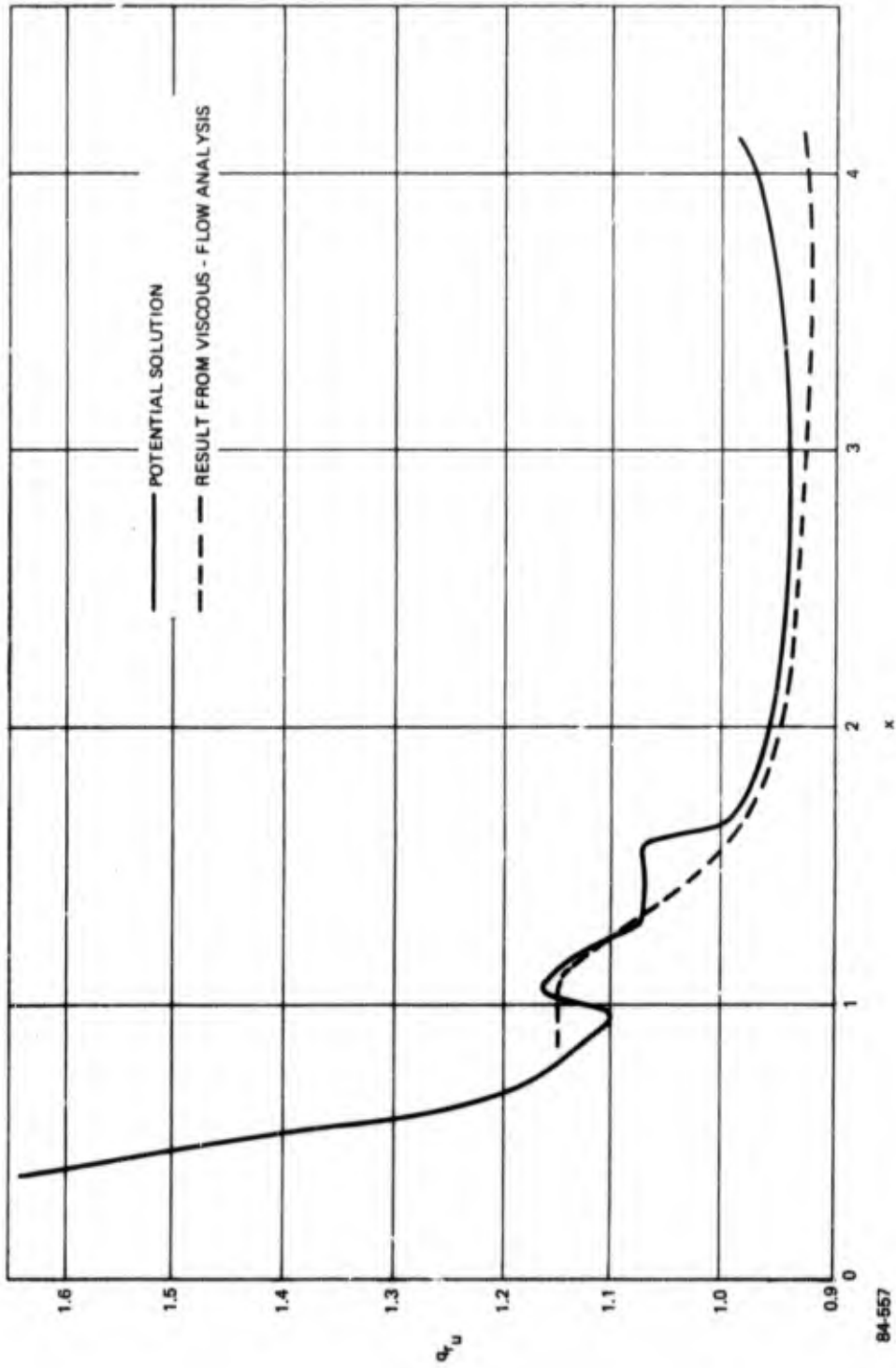


Figure 8 LIFT COEFFICIENT VARIATION DURING OSCILLATORY PITCHING AT A REDUCED FREQUENCY OF 0.1



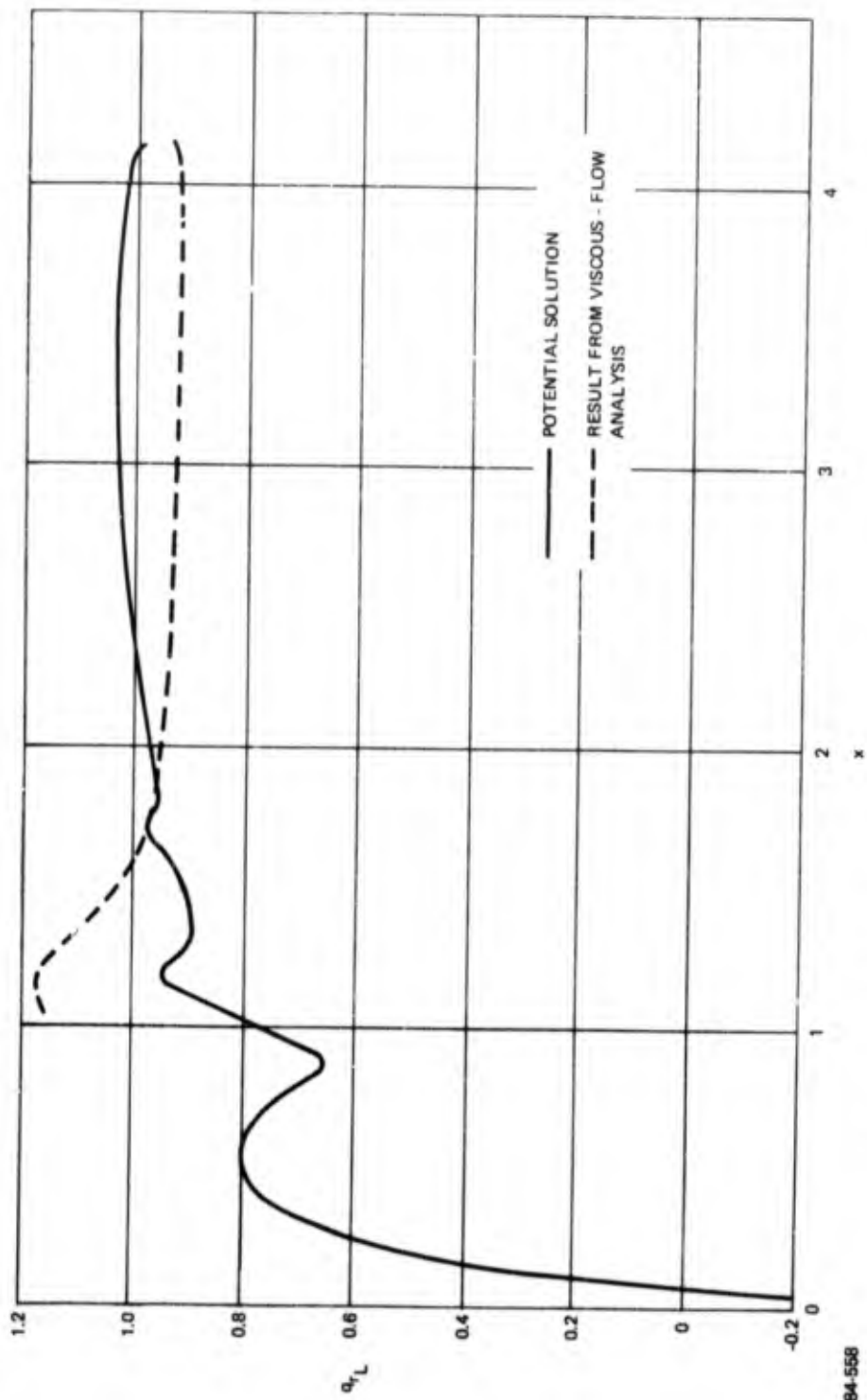
84-556

Figure 9 BOUNDARY OF POTENTIAL FLOW WITH SEPARATION AT $x = 0.75$, $\gamma = 2$, $a_b = 0.41$



84-557

Figure 10 MAGNITUDE OF FLUID VELOCITY ON UPPER SURFACE OF AIRFOIL AND SHEAR LAYER WITH SEPARATION AT $x = 0.75$, $\gamma = 2$, $\theta_b = 0.41$



84-556

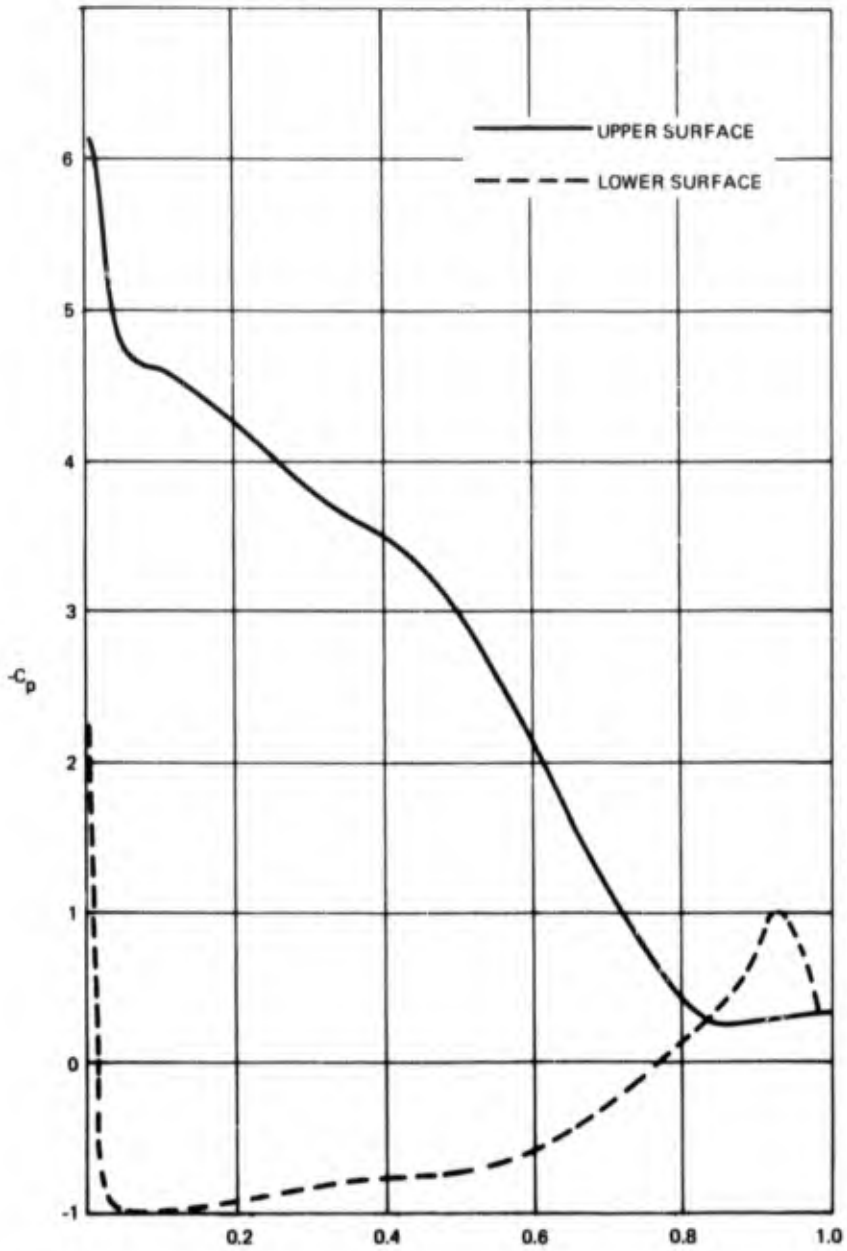
Figure 11 MAGNITUDE OF FLUID VELOCITY ON LOWER SURFACE OF AIRFOIL AND SHEAR LAYER WITH SEPARATION AT $x = 0.75$, $\gamma = 2$, $\alpha_0 = 0.41$

as much as 10% in the pressure recovery and wake regions. While it is not possible to definitely affix the blame for the failure of this approach without an actual solution available for comparison, it would appear, in retrospect, that the basic premise under which the surface enclosing the separated region was defined is not valid. While displacement thickness does provide a reasonable measure of the effect of a boundary layer on the external flow, the use of that parameter directly, in this problem, to account for the lateral extent of a region with a substantial amount of reversed flow is definitely open to question.

As noted in Section 4, a reasonable solution for steady flow was obtained by imposing a boundary condition on pressure along the upper surface between the separation point and the trailing edge and along the streamline emanating from the trailing edge. The chordwise pressure distribution obtained, for an angle of attack of .2 rad., with the separation point at $x = .85$ (no iteration on separation point location was performed) is shown in Figure 12. The iteration on flow direction between $x = .85$ and $x = 1$ converged in five steps.

When the method was applied to a case of transient pitching through stall, the iteration on flow direction diverged. The problem appeared to be centered at the trailing edge so the Kutta condition was modified as described in Section 4. No improvement in the situation was obtained by that change. The number of source elements in the vicinity of the trailing edge was then substantially increased. Convergence of the iteration on flow direction was then obtained for the separation point located at $x = .85$. However, on the next iteration, with the separation point at $x = .9$, the iteration on flow direction again diverged.

It does appear that a valid solution could eventually be obtained. However, a great deal of effort would be required to overcome the severe numerical difficulties encountered. On the other hand, imposition of a linearized pressure condition was found, in Ref. 18, to give quite reasonable results from a qualitative standpoint for both leading edge and trailing edge stall. A more tractable means of achieving the original objectives of the study would seem, then, to be through systematic refinement of the linearized formulation, rather than by a direct attack on the complete nonlinear problem. Specifically, it is recommended that second-order terms be derived through Taylor series expansions of the potential and the boundary conditions, paralleling the approach taken by Lighthill in Ref. 26 for the problem of steady attached flow.



84-559 Figure 12 CHORDWISE PRESSURE DISTRIBUTION OBTAINED WITH
BOUNDARY CONDITION ON PRESSURE - SEPARATION
AT $x = 0.85$

6.0 REFERENCES

1. Ham, N. D. and Young, M. I., "Torsional Oscillation of Helicopter Blades Due to Stall," *J. Aircraft*, Vol. 3, No. 3, May-June 1966, pp. 218-224.
2. Emmons, H. W., Kronauer, R. E., and Rockett, J. A., "A Survey of Stall Propagation-Experiment and Theory," *J. of the ASME, J. of Basic Eng. (Series D)*, Vol. 31, Sept. 1959, pp. 409-416.
3. Schnittger, J. R., "Single Degree of Freedom Flutter of Compressor Blades in Separated Flow," *J. Aero. Sci.*, Vol. 21, No. 1, Jan. 1959, pp. 27-36.
4. Halfman, R., Johnson, H. and Haley, S., "Evaluation of High Angle-of-Attack Aerodynamic-Derivative Data and Stall-Flutter Prediction Techniques," NACA TN 2533, Nov. 1951.
5. Sisto, F., "Stall-Flutter in Cascades," *J. Aero. Sci.*, Vol. 20, No. 9, Sept. 1953, pp. 598-604.
6. Liiva, J., Davenport, F., Gray, L. and Walton, I., "Two-Dimensional Tests of Airfoils Oscillating Near Stall -- Vol. I, Summary and Evaluation of Results," USAVLABS Tech. Rept. 68-13A, April 1968.
7. Velkoff, H., Blaser, D. and Jones, K., "Boundary-Layer Discontinuity on a Helicopter Rotor Blade in Hovering," *J. Aircraft*, Vol. 8, No. 2, February 1971, pp. 101-107.
8. Dwyer, H. A. and McCroskey, W. J., "Crossflow and Unsteady Boundary-Layer Effects on Rotating Blades," *AIAA J.*, Vol. 9, No. 8, August 1971, pp. 1498-1505.
9. McCroskey, W. J. and Fisher, R. K., "Detailed Aerodynamic Measurements on a Model Rotor in the Blade Stall Regime," *J. Am. Helicopter Soc.*, Vol. 17, No. 1, January 1972, pp. 20-30.
10. Martin, J. M., Empey, R. W., McCroskey, W. J., and Caradonna, F. X., *Am. Helicopter Soc. Preprint No. 702*, May 1973.
11. Patay, S. A., "Leading Edge Separation on an Airfoil During Dynamic Stall," M.I.T. ASRL TR 156-1, October 1969.

12. Woods, L. C., "Aerodynamic Forces on an Oscillating Airfoil Fitted with a Spoiler," Proc. Roy. Soc., Series A, Vol. 239, 1957, pp. 328-337.
13. Ham, N. D., "Aerodynamic Loading on a Two-Dimensional Airfoil During Dynamic Stall," AIAA J., Vol. 6, No. 10, October 1968, pp. 1927-1934.
14. Ericsson, L., and Reding, J., "Unsteady Airfoil Stall," NASA CR-66787, July 1969.
15. Carta, F. and Neibanck, C., "Prediction of Rotor Instability at High Forward Speeds - Vol. III, Stall Flutter," USAAVLABS TR 68-18C, February 1969.
16. Tarzanin, F. J., "Prediction of Control Loads Due to Blade Stall," J. Am. Helicopter Soc., Vol. 17, No. 2, April 1972.
17. Crimi, P. and Reeves, B. L., "A Method for Analyzing Dynamic Stall of Helicopter Rotor Blades," NASA CR-2009, May 1972.
18. Crimi, P., "Investigation of Nonlinear Inviscid and Viscous Flow Effects in the Analysis of Dynamic Stall," NASA CR-2335, February 1974.
19. Giesing, J. P., "Nonlinear Two-Dimensional Unsteady Potential Flow with Lift," J. Aircraft, Vol. 5, No. 2, March-April 1968, pp. 135-143.
20. McCullough, G. B., and Gault, D. E., "Examples of Three Representative Types of Airfoil-Section Stall at Low Speed," NACA TN 2502, September 1951.
21. Ward, J. W., "The Behavior and Effects of Laminar Separation Bubbles on Airfoils in Incompressible Flow," J. Roy. Aero. Soc., Vol. 67, December 1963, pp. 783-790.
22. Schlichting, H., Boundary Layer Theory, Fourth Edition, McGraw-Hill, New York, 1960.
23. Sears, W. R. and Telionis, D. P., "Unsteady Boundary-Layer Separation," Preprint, IUTAM Symposium on Unsteady Boundary Layers, Quebec, May 1971.
24. Klineberg, J. M. and Lees, L., "Theory of Laminar Viscous-Inviscid Interactions in Supersonic Flow," AIAA Paper 69-7, January 1969.

25. Reeves, B. L. and Lees, L., "Theory of Laminar Near Wake of Blunt Bodies in Hypersonic Flow," AIAA J., Vol. 3, No. 11, November 1965, pp. 2061-2074.
26. Lighthill, M. J., "A New Approach to Thin Airfoil Theory," Aeron. Quart., Vol. 3, November 1951, pp. 193-210.

APPENDIX

Functions Defining Contributions to Flow Components and Potential at Element i

$$u_{ij} = \hat{q}_x c_{\beta j} - \hat{q}_y s_{\beta j}$$

$$v_{ij} = \hat{q}_y c_{\beta j} + \hat{q}_x s_{\beta j}$$

$$\phi_{ij} = (l_j - \hat{x}) \ln r_B^2 + \hat{x} \ln r_A^2 + 2\hat{y} \psi$$

where, with the coordinates of the end points of element i denoted (x_i, y_i) and (x_{i+1}, y_{i+1}) ,

$$\bar{x}_i = \frac{1}{2}(x_{i+1} + x_i), \quad \bar{y}_i = \frac{1}{2}(y_{i+1} + y_i)$$

$$l_j = \left[(x_{j+1} - x_j)^2 + (y_{j+1} - y_j)^2 \right]^{1/2}$$

$$s_{\beta j} = (y_{j+1} - y_j)/l_j, \quad c_{\beta j} = (x_{j+1} - x_j)/l_j$$

$$\hat{x} = (\bar{x}_i - x_j) c_{\beta j} + (\bar{y}_i - y_j) s_{\beta j}$$

$$\hat{y} = (\bar{y}_i - y_j) c_{\beta j} - (\bar{x}_i - x_j) s_{\beta j}$$

$$r_A^2 = \hat{x}^2 + \hat{y}^2, \quad r_B^2 = (\hat{x} - l_j)^2 + \hat{y}^2$$

$$\psi = \tan^{-1} \left(\frac{\hat{x}}{\hat{y}} \right) - \tan^{-1} \left(\frac{\hat{x} - l_j}{\hat{y}} \right)$$

$$\hat{q}_x = \ln \left(\frac{r_A}{r_B} \right), \quad \hat{q}_y = \psi$$

$$u_{\Gamma_i} = -6 \bar{y}_i + 3 \bar{y}_i (1 - 2 \bar{x}_i) f_L \\ + 6 \left[\bar{x}_i (1 - \bar{x}_i) + \bar{y}_i^2 \right] f_A$$

$$v_{\Gamma_i} = 3 - 6 \bar{x}_i + 3 \left[\bar{x}_i (1 - \bar{x}_i) + \bar{y}_i^2 \right] f_L - 6 \bar{y}_i (1 - 2 \bar{x}_i) f_A$$

$$\theta_{\Gamma_i} = 2 \bar{y}_i (1 - 2 \bar{x}_i) + \bar{y}_i \left[3 \bar{x}_i (1 - \bar{x}_i) + \bar{y}_i^2 \right] f_L \\ + \left[\bar{x}_i^2 (3 - 2 \bar{x}_i) - 3 \bar{y}_i^2 (1 - 2 \bar{x}_i) \right] f_A$$

where

$$f_L = \ln \left[\frac{(1 - \bar{x}_i)^2 + \bar{y}_i^2}{\bar{x}_i^2 + \bar{y}_i^2} \right]$$

$$f_A = \tan^{-1} \left(\frac{\bar{x}_i}{\bar{y}_i} \right) - \tan^{-1} \left(\frac{\bar{x}_i - 1}{\bar{y}_i} \right)$$

while

$$u_{\gamma_i} = 3 \bar{y}_i + \bar{y}_i (3 \bar{x}_i - 1) f_L + \left[\bar{x}_i (3 \bar{x}_i - 2) - 3 \bar{y}_i^2 \right] f_A$$

$$v_{\gamma_i} = 3 \bar{x}_i - \frac{1}{2} + \frac{1}{2} \left[\bar{x}_i (3 \bar{x}_i - 2) - 3 \bar{y}_i^2 \right] f_L - 2 \bar{y}_i (3 \bar{x}_i - 1) f_A$$

$$\theta_{\gamma_i} = \frac{\bar{y}_i}{2} (4 \bar{x}_i - 1) + \frac{\bar{y}_i}{2} \left[\bar{x}_i (3 \bar{x}_i - 2) - \bar{y}_i^2 \right] f_L \\ + \left[\bar{y}_i^2 (1 - 3 \bar{x}_i) - \bar{x}_i^2 (1 - \bar{x}_i) \right] f_A$$

$$u_{\gamma_{s_1}} = 2 \bar{y}_i (2 \bar{x}_i - 1) + (1 - 2 \bar{x}_i) \left[\bar{x}_i (1 - \bar{x}_i) + \bar{y}_i^2 \right] f_A \\ - \frac{1}{2} \bar{y}_i \left[6 \bar{x}_i (1 - \bar{x}_i) - 1 + 2 \bar{y}_i^2 \right] f_L$$

$$v_{\gamma_{s_1}} = \frac{1}{6} - 2 \bar{x}_i + 2 (\bar{x}_i^2 - \bar{y}_i^2) + \bar{y}_i \left[6 \bar{x}_i (1 - \bar{x}_i) - 1 + 2 \bar{y}_i^2 \right] f_A \\ + \frac{1}{2} (1 - 2 \bar{x}_i) \left[\bar{x}_i (1 - \bar{x}_i) + 3 \bar{y}_i^2 \right] f_L$$

$$\emptyset_{\gamma_{s_1}} = \frac{\bar{y}_i}{2} \left[\frac{1}{3} - 3 \bar{x}_i (1 - \bar{x}_i) - \bar{y}_i^2 \right] \\ + \left\{ \frac{\bar{x}_i^2}{2} (1 - \bar{x}_i)^2 + \bar{y}_i^2 \left[3 \bar{x}_i (1 - \bar{x}_i) - \frac{1}{2} (1 - \bar{y}_i^2) \right] \right\} f_A \\ + \frac{\bar{y}_i}{2} (1 - 2 \bar{x}_i) \left[\bar{y}_i^2 + \bar{x}_i (1 - \bar{x}_i) \right] f_L$$

$$u_{\gamma_{s_2}} = 4 \bar{y}_i \left[15 G^2 - 20 \bar{y}_i^2 - 13/3 \right] \\ + s_1 f_A - s_2 f_L$$

$$v_{\gamma_{s_2}} = 10 G^3 - 120 G \bar{y}_i^2 - 26 G/3 \\ + 2 s_2 f_A + \frac{1}{2} s_1 f_L$$

$$\emptyset_{\gamma_{s_2}} = \bar{y}_i G (8 G^2 - 20/3 - 32 \bar{y}_i^2) \\ + \frac{G}{2} \left[(1 - G^2 + 4 \bar{y}_i^2)^2 + 16 \bar{y}_i^2 (1 - 2 \bar{x}_i^2 + 4 \bar{y}_i^2) \right] f_A \\ + \frac{\bar{y}_i}{2} \left[(1 - G^2 + 4 \bar{y}_i^2)^2 - 4 G^2 (1 - G^2 + 8 \bar{y}_i^2) \right] f_L$$

where

$$G = 2 \bar{x}_i - 1$$

$$s_1 = 4 \bar{y}_i G (3 - 5 G^2 + 20 \bar{y}_i^2)$$

$$s_2 = (1 - G^2 + 4 \bar{y}_i^2) (1 - 5 G^2 + 20 \bar{y}_i^2) - 80 \bar{y}_i^2 G^2$$

If wake element k has end points (x_k, y_k) and (x_{k+1}, y_{k+1}) , and strengths γ_k and γ_{k+1} , respectively, at those end points, then:

$$u_{wik} = q_{xw} c_{\beta k} - q_{yw} s_{\beta k}$$

$$v_{wik} = q_{yw} c_{\beta k} + q_{xw} s_{\beta k}$$

where

$$q_{xw} = \frac{1}{2} (\gamma_{k+1} - \gamma_k) \frac{\hat{y}}{l_k} L + \left[\gamma_k + (\gamma_{k+1} - \gamma_k) \frac{\hat{x}}{l_k} \right] \psi$$

$$q_{yw} = \gamma_{k+1} - \gamma_k + \frac{1}{2} \left[\gamma_k + (\gamma_{k+1} - \gamma_k) \frac{\hat{x}}{l_k} \right] L$$

$$- \frac{\hat{y}}{l_k} (\gamma_{k+1} - \gamma_k) \psi$$

in which $L = \ln \left(\frac{r_B^2}{r_A^2} \right)$

while other quantities are as defined previously.